Appl. Phys. B 78, 249–256 (2004)
DOI: 10.1007/s00340-003-1358-5

Applied Physics B
Lasers and Optics

R. JIMÉNEZ[1]
M. TASLAKOV[1]
V. SIMEONOV[1,✉]
B. CALPINI[1,*]
F. JEANNERET[1]
D. HOFSTETTER[2]
M. BECK[2]
J. FAIST[2]
H. VAN DEN BERGH[1]

Ozone detection by differential absorption spectroscopy at ambient pressure with a 9.6 μm pulsed quantum-cascade laser

[1] Air Pollution Laboratory (LPAS), Swiss Federal Institute of Technology (EPFL), 1015 Lausanne, Switzerland
[2] Institute of Physics, University of Neuchâtel, Breguet 1, 2000 Neuchâtel, Switzerland

Received: 21 July 2003/Revised version: 29 September 2003
Published online: 10 December 2003 •

ABSTRACT We report direct absorption spectroscopic detection of ozone at ambient pressure with a pulsed, DFB quantum-cascade laser (QCL) tuned within 1044–1050 cm^{-1} by temperature scanning. Wavelength calibration curves were derived from FTIR and CO_2 spectra and interpreted with respect to the heat transfer from the heterostructure to the sink. The laser linewidth ($\sim 0.13\ cm^{-1}$ FWHM) was found to decrease with temperature, probably as a result of operation at constant current. Spurious spectral features due to baseline inaccuracies were successfully filtered out from the QCL O_3 spectra using differential absorption. Reference O_3 concentrations were obtained by applying the same method to UV spectra, simultaneously measured with a differential optical absorption spectrometer (DOAS). Column densities retrieved from QCL spectra are in fairly good agreement (±20%) with the DOAS values above 28 ppm m. The estimated QCL lowest detectable, absolute and differential absorptions, (7×10^{-3} and 2×10^{-3}, respectively), entail effective detection limits of 14 and 25 ppm m, respectively. Ongoing improvements in the acquisition system should allow the achievement of detection limits at the level of commercial open-path DOAS systems (~ 2 ppm m) in the near future. Our results demonstrate the applicability of the differential absorption method to QCL spectroscopy at ambient pressure, and encourage its use for open path detection.

PACS 42.62.Fi; 82.80.Gk; 92.60.Sz

1 Introduction

The understanding and mitigation of complex air pollution phenomena requires the application of elaborated finite volume models, which are typically run with a horizontal resolution of $\sim$ 1–5 km for urban areas [1–3]. This averaged description of the atmosphere entails validation measurements of similar spatial resolution. Ground level point measurements frequently lack representativeness for this purpose, particularly in poorly mixed atmospheres [4]. On the contrary, optical remote sensing techniques [5], such as DOAS [6, 7], open-path (OP) FTIR and TDLAS, provide directly space-averaged concentrations of various trace gases. These spectroscopic techniques have nevertheless intrinsic limitations: DOAS is restricted to the few species that have relatively narrow, highly structured transition bands in the UV-visible. Compactness required to OP-FTIR systems usually implies low spectral resolution, which limits its selectivity. Achievable absorption paths are usually short (< 200 m) as well, which may lead to low sensitivity. Mid-IR TDLAS systems operate at high spectral resolution but are hardly tunable and require cryogenic cooling.

The advent of the quantum-cascade laser (QCL) in 1994 [8], and its rapid development during the last years [9], has opened up the possibility of using tunable, non-cryogenic, narrow linewidth sources for real-time spectroscopic monitoring of a large number of molecular species in the mid-IR, particularly in the 3–5 μm and 8–13 μm H_2O atmospheric windows. QCL-based point measurements of several trace gases have been successfully demonstrated during the last years [10–16]. With few exceptions [14–16], these measurements have been performed at low pressure and in closed, folded optical path systems (e.g. White or Herriott cells) for sensitivity improvement. Extractive ambient air measurements are obviously local and have the disadvantage of requiring sample manipulation, which frequently leads to undesirable wall and reaction effects. The signal-to-noise ratio (SNR) reduction due to broadening of the rovibrational bands at ambient pressure can however be compensated by using long open paths. Regarding, for example the detection of O_3 at ~ 9.6 μm, the absorption levels obtained with a 100 m multiple-reflection cell operated at 10 mbar could be achieved as well with an $\sim$ 1.8 km atmospheric path arrangement.

Our research aims to exploit the advantages of the QCL for the detection of relevant trace gases using long open atmospheric paths. One intrinsic advantage of measuring in the mid-IR is that detection is not affected by the presence of aerosols, in contrast with UV-visible systems (DOAS). The rapid progress in the mid-IR detection technology is expected to allow field-deployable, fully non-cryogenic operation in the near future. Currently available pyroelectric detectors are limited in bandwidth (< 2 kHz) [12], and as shown in the last section, appear not yet suitable for open-path applications.

In order to simulate open-air conditions in the laboratory, we performed direct absorption spectroscopic measurements of O_3 at ambient pressure using a flow system. In addition to

✉ Fax: +41-21/693-5145, E-mail: valentin.simeonov@epfl.ch
*_Present address_: MeteoSwiss, 1530 Payerne, Switzerland

its relevance in tropospheric air pollution and global warming, we chose ozone as the test compound because: (1) the QCL available spectral range (1040–1050 cm^{-1}) is within the strong υ_3 vibrational band [17]; (2) accurate O_3 monitoring techniques (UV DOAS and photometric point analyzers) are available, which allows for reliable laboratory calibration and future intercomparison in open path conditions.

2 Experimental setup

A schematic of the experimental setup is shown in Fig. 1. The quantum-cascade laser (QCL) used is an InGaAs-AlInAs/InP distributed feedback (DFB) commercial prototype (Alpes Lasers, DFB-QCL) devised for pulsed operation (Alpes Lasers, TPG 128 and LDD 100-pulse timer and switcher, respectively) at near room temperature with a characteristic emission wavelength of $\sim 1046.9\,cm^{-1}$ ($\sim$ 9.55 μm) at 0 °C tunable at $\sim -7.5 \times 10^{-2}\,cm^{-1}$/K from −40 to +80 °C (see next section for calibration details). A tap water-sink Peltier-based thermal management system allows controlling the QCL temperature within ±0.1 °C. Measured average power at −30 °C reaches 5.7 mW operating at 2.25% duty cycle (dc) with 6.9 A (peak current) pulses at 9.6 V (bias voltage). Slow temperature-scanning spectroscopic measurements were performed with the QCL emission driven by 50 ns electrical pulses (6 A/8 V) repeated at 100 or 300 kHz (0.5 and 1.5% dc, respectively).

A 10.6 μm-optimized antireflection (AR)-coated, aspheric ZnSe lens (∅ 28 mm, $f = 25$ mm) was employed to collimate the highly divergent, far field elliptical QCL beam ($\sim 60°$ vertical, $\sim 40°$ horizontal). A 3 mm thick, AR-coated ZnSe beam splitter allowed the use of a 532 nm Nd : YAG beam coaxial to the mid-IR beam for alignment purposes. The QCL beam was directed into the absorption cell using a flat Al mirror (M1). The cell is a plain aluminum profile (100 × 9 × 4 cm) equipped with tight window frames, a 3 mm tick AR ZnSe window (∅ 25 mm), and a Au-coated, path-folding mirror (FM) placed inside the cell. After a double pass along the cell ($L = 192$ cm - effective absorption pathlength), the QCL beam is directed (using the Al mirrors M1 and M2) to a spherical Al mirror (M3: ∅ 50 mm, $f = 1$ m), which finally focuses it onto a fast response (25 ns rise time), liquid nitrogen cooled HgCdTe (MCT) photovoltaic detector (Kolmar Technologies, KMPV11-1-J1/DC - 0.8 mm^2 active area, 60° angle of view, peak responsivity at 10.1 μm, 50 MHz built-in amplifier). The detector window was masked with a ∅ 2 mm pinhole in order to reduce the effect of background radiation sources. MCT signals were acquired with a 500 MHz, 8-bit digital oscilloscope (LeCroy, 9354 AL) triggered by the QCL electric driving pulse. For temperature scanning purposes, the QCL temperature controller (Alpes Lasers, TC-51) was externally driven with a 16-bit digital-to-analog converter (DAC) computer card (ADLink, PCI-6208V). The TC-51 actual temperature analog signal was digitized using a multimeter (Fluke, 8842A) and then gathered via GPIB by a LabView® data acquisition/scanning manager program. Temperature scans were performed bi-directionally, typically at 10–15 mK steps. This very slow scanning rate assures an almost perfectly monotonic, ripple-free linear temperature slope. A unidirectional 70 K scan takes typically $\sim$ 20 min. The QCL signal amplitude is software-calculated by subtracting the MCT signal baseline (last $\sim$ 100 data points) from the pulse peak average intensity ($\sim$ 10 data point around the pulse maximum). Due to software and instrument communication limitations, only $\sim$ 5 pulses per temperature step were actually acquired.

A closed circuit flow configuration was used for the ozone measurements. Previously, for every experimental run, high purity oxygen (SL Gas, $O_2 > 99.9995\%$) was introduced into the circuit until achieving full purge of the system through the exhaust line. Baseline spectra were then recorded. Subsequently, a homemade oxygen photolyzer equipped with three low-pressure Hg lamps was used to build up and sustain at steady-state various ozone concentrations (1–700 ppm). Absorption spectra were then recorded. The concentration of ozone inside the cell was real-time monitored using a differential optical absorption spectrometer (Thermo Electron Air Quality, DOAS 2000) and a calibrated UV-photometric point monitor (Dasibi, 1008-RS 1 ppb lower detection limit -LDL). The point analyzer was utilized for monitoring low ozone concentrations (< 2 ppm) only, in particular to check the attainment of full purging of the cell with O_2. In addition, its pump served to keep a constant flow (1.5 L/min) through the gas circuit. The flow conditions were real-time monitored using a Pt-100 thermometer and a pressure transducer (Setra, 280E) linked to a 10-bit datalogger (Texas Electronics, Solus).

The DOAS beam was obtained by collimation of light from a 150 W high-pressure Xe lamp (Hamamatsu, L2274). After a single pass through the cell (1 m absorption path length), the beam is focused onto a 19-optical-fiber bundle connected to a $f/3.9$ (0.2 m) Czerny–Turner spectrometer equipped with a 600 groove/mm ruled grating. The diffracted beam is linearly scanned at 30 Hz by a miniature electromechanically-swept slit and detected by a side-on PMT. The scanner position is quasi-real-time mapped by a diode laser/etched photocell system perpendicular to detection plane. A transmitted intensity-controlled, automatic grating positioning routine was developed in order to measure O_3 over a large concentration span at optimum SNR conditions. In this way, the highest concentrations were measured in the 300–330 nm range and the lowest at 247–277 nm (Hartley band maximum). The first wavelength range assures

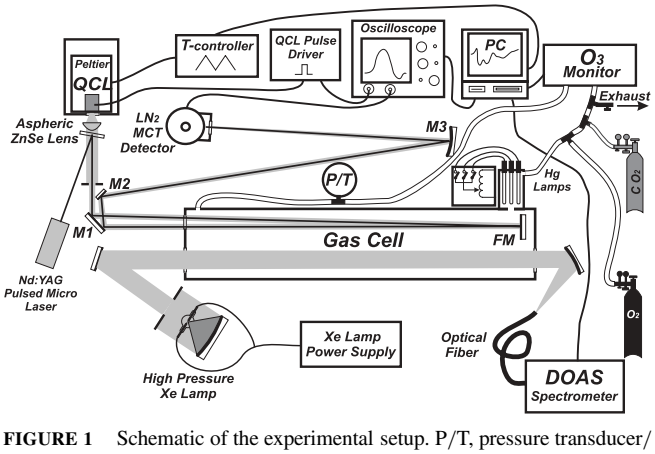

FIGURE 1 Schematic of the experimental setup. P/T, pressure transducer/temperature indicator

that transmitted intensities are high enough to be properly detected, and the second one, that the highest possible absorption is attained. The reference O_3 concentrations were retrieved by non-linear fitting of the DOAS spectra to a high resolution cross section [18], previously convolved with the spectrometer function (0.56 nm FWHM). The implemented differential spectra fitting algorithm is similar to the one developed by Stutz and Platt [7]. Based on laboratory measurements, the DOAS LDL (3-sigma) in the 247–277 nm range at the minimum QCL spectra scanning/co-adding total time ($\geq$ 1 h) is estimated to be lower than 0.74 ppm m (the LDL at 2 min integration time is 2.7 ppm m). The retrieved concentrations are precise, within ±3% on average. Since both DOAS and QCL are based on optical absorption, full comparability between the two systems is assured, even if minor concentration gradients could develop along the cell.

3 Wavelength calibration and linewidth estimation

We obtained transmission spectra by slow temperature scanning. Appropriate spectral mapping of these scans requires accurate knowledge of the laser wavelength dependence on temperature at various operational conditions. We measured this dependence using a low resolution (0.5 cm^{-1} FWHM) FTIR spectrometer (Nicolet 800), and through CO_2 spectra measured at ambient pressure, displayed four well resolved $00^01 \leftarrow 02^00$, 9P-branch rovibrational transitions ($P18$, $P20$, $P22$, $P24$) [19] (see Fig. 2a). High purity carbon dioxide (SL Gas, $CO_2 > 99.998\%$) spectra were acquired using bi-directional temperature scanning within −35 to +50 °C with the QCL excited with 50 ns electric pulses repeated at 100 or 300 kHz (0.5% or 1.5% dc, respectively).

The QCL heat sink temperatures (T_S) at the CO_2 broadened absorption transition maxima, $T_{S,k}$, were determined with a precision better than ±0.2 K (±0.015 cm^{-1} equivalent uncertainty). We observed statistically significant differences in $T_{S,k}$, of up to −0.6 K, between subsequent cooling-down and heating-up scanned CO_2 spectra. These small differences and the significant differences observed between CO_2 spectra measured at 0.5% and 1.5% dc ($\Delta T_{S,k} \approx -4.4$ K – see Fig. 2a) are explained by the increase of the heterostructure-to-sink temperature gradient with an increase of the heat dissipated by the laser. The slight decrease with temperature of the overall heat transfer coefficient explains why the wavelength calibration slope decreases with increasing power duties as observed in Fig. 2b. Calibration curves are appropriately described by first-degree fitting polynomials. Before linear fitting of the ($T_{S,k}$, $\tilde{\nu}_k$) data pairs, the temperature-scanned CO_2 spectra were co-added and averaged, baseline subtracted, low-pass filtered (Savitzky–Golay), and the peak absorption temperatures ($T_{S,k}$) determined at the optical density local maxima. We took care of preserving separate calibration curves for heating-up and cooling-down scanned spectra in order to account for minute differences as explained above. The wavelength accuracy, estimated as the maximum calibration residual, is better than ±0.03 cm^{-1}.

Appropriate comparison of our experimental spectra with HITRAN-based [20] calculations requires estimation of the QCL linewidth. For this purpose, the observed CO_2 transition lines were separately fitted to a model lineshape and analyzed. As expected, at atmospheric pressure, the observed lines were found to best fit to a Lorentzian lineshape. Supported by convolution calculations that achieved reproduction of the FTIR observations, we assumed the QCL emission lineshape to be Lorentzian as well. This assumption allows estimating the QCL halfwidth ($\alpha_{L,QCL}$) by subtraction of the HITRAN-based calculated transitions halfwidths ($\alpha_{L,\sigma}$) from the observed halfwidths ($\alpha_{L,D} \cong \alpha_{L,\sigma} + \alpha_{L,QCL}$). This approach has been widely used for linewidth estimation [12, 15, 21]. The retrieved QCL halfwidths at 0.5% dc range from 0.056 cm^{-1} for the $P22$ transition to 0.067 cm^{-1} for the $P18$ (1.7–2.0 GHz). These linewidths are narrower

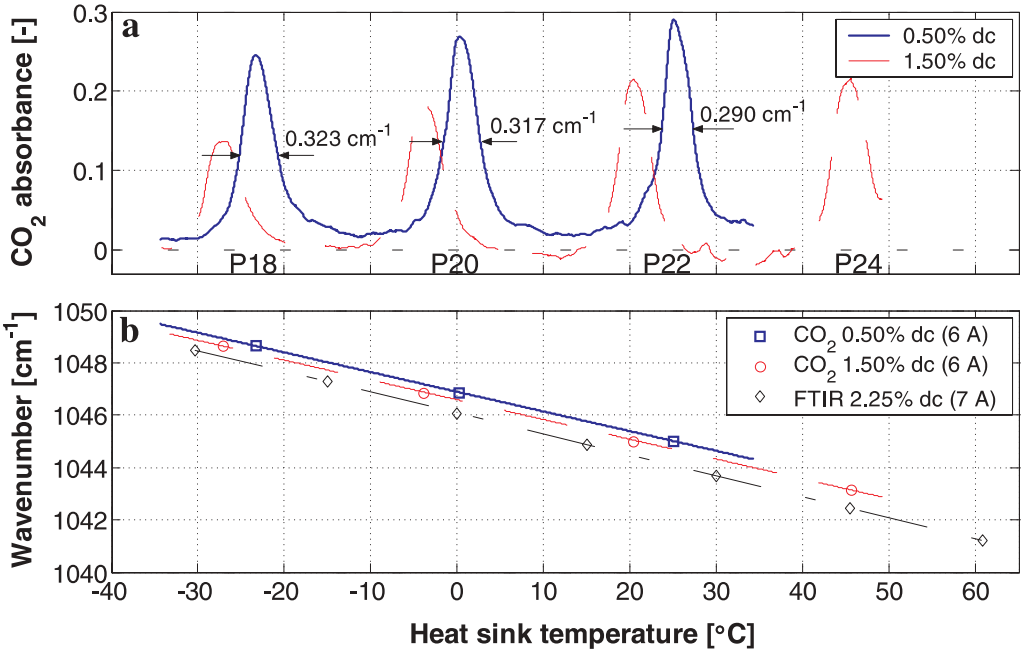

FIGURE 2 QCL wavelength and linewidth. **a** Temperature-scanned CO_2 absorption spectra at two duty cycles and at constant current (6 A). The observed $00^01 \leftarrow 02^00$, 9P-branch rovibrational transitions are indicated along with their linewidths. **b** CO_2- and FTIR-derived wavelength calibration curves at various duty cycles (dc) and peak currents

than expected for a 50 ns long pulse [14, 15], and show negative dependence with the heat sink temperature. Retrieved linewidths at 1.5% dc and FTIR spectra show a similar behavior. Our findings are apparently in contradiction with recent theoretical calculations that state positive dependence of the QCL linewidth with temperature [22, 23]. These calculations refer nevertheless to isothermal operation at a constant current (i) above the lasing threshold current (i_{th}). We obtained spectra by slow temperature scanning over a fairly large range, operating at fixed current, and thus at a variable i/i_{th} ratio. As a consequence, one can expect broader linewidths at lower temperatures for which the threshold current is smaller, thus the i/i_{th} ratio is higher. This may explain our experimental observations.

4 Absolute and differential analysis of ozone spectra

Ozone absorption spectra at seven steady-state concentration levels within 1–631 ppm were acquired by bi-directional scanning of the QCL at 0.5% dc from −35 to +35 °C (1044–1050 cm^{-1}). In this wavelength range, ozone displays the highly structured R-branch of its 001 ← 000 vibrational band [17] (O_3 is a greenhouse gas largely because of the infrared absorption in this band). Six to 45 absorption spectra were scanned per O_3 level. Baseline, $I_0\,(T_{\mathrm{S}})$, and absorption scans, $I\,(T_{\mathrm{S}})$, were logarithmically averaged. The average optical density, $\overline{D}$, was calculated as the average $\overline{\ln\,(I)}$ subtracted from the average $\overline{\ln\,(I_0)}$. Heating-up and cooling-down spectra were separately averaged and temperature-to-wavenumber transformed. The resulting absorption spectra are shown in the Fig. 3 along with their corresponding theoretical optical densities (D_{H}),

$$D_{\mathrm{H}}\,(\tilde{\nu}) = -\ln\left[\tau_{\mathrm{H}}\,(\tilde{\nu})\right] \qquad (1)$$

calculated using the DOAS-retrieved ozone concentrations (c). The theoretical transmittances, $\exp\,(-\sigma cL)$, were convolved with a Lorentzian QCL emission lineshape (H) of constant width, taken as the average halfwidth retrieved from the CO_2 spectra ($\overline{\alpha}_{\mathrm{L,QCL}} = 0.063\ \mathrm{cm}^{-1}$),

$$\tau_{\mathrm{H}}\,(\tilde{\nu}) = \exp\left[-\sigma\,(\tilde{\nu})\,cL\right] \otimes H\left(\tilde{\nu}'\right). \qquad (2)$$

τ_{H} is the convolved theoretical transmittance, σ is the HITRAN-based calculated (pressure, temperature-dependent) absorption cross section [20], and L is the absorption path length (cL is the column density).

The common-baseline absorption spectra displayed in Fig. 3a ($cL > 300$ ppm m) show consistently lower optical densities than that expected from the BLB law. This discrepancy stems from underestimation of the baseline level, probably due to optical misalignment. Calculated spectra in this panel also show excessive spectral smoothing at the lower wavenumbers. This points to a narrower-than-average QCL emission linewidth at the lower wavenumbers and provides additional evidence of the inverse linewidth-to-temperature dependence behavior.

At column densities below 80 ppm m (see Fig. 3b), the relative difference between baseline and transmitted intensity, i.e. the absorptivity $(1 - \tau_{\mathrm{H}})$, becomes smaller than ∼ 5%. At these absorption levels, relatively small baseline deviations can cause spurious, broad features in the optical density spectra, particularly within the lower absorption range ($\tilde{\nu} < 1046\ \mathrm{cm}^{-1}$). The effect of an inaccurately defined baseline on atmospheric pressure absorption spectra is particularly noticeable on the 28 ppm m spectrum shown in Fig. 4a, which is apparently in poor agreement with the HITRAN-based calculated optical densities. The concentration retrieval in this situation can be largely improved using the differential absorption approach. In this approach, distinction is made between 'broad' and 'narrow' spectral variations [6, 7]. The narrow variations are extracted from the absorption spectra by simple subtraction of a synthetic, smooth trend curve, $f\,(D)$. This low-pass (LP) filter represents the broadband spectral component and is defined by the absorption spectra itself so no

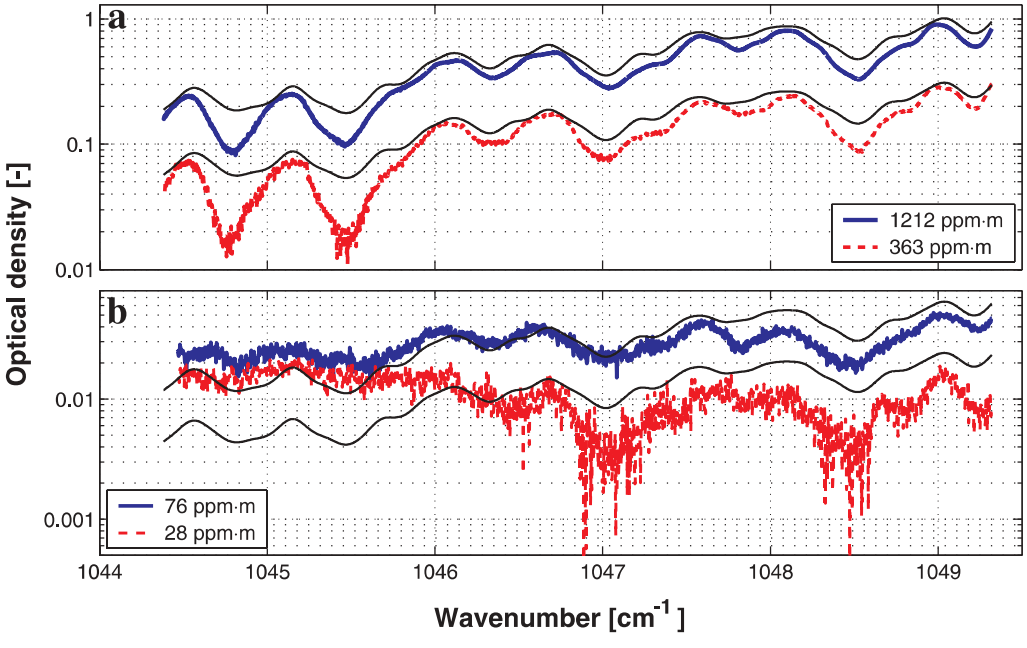

FIGURE 3 Measured *(thick lines)* and HITRAN-based calculated *(thin lines)* QCL absorption spectra at **a** high/moderate and **b** low O_3 column densities over a 192 cm long effective absorption path. Discrepancies mainly stem from baseline inaccuracies

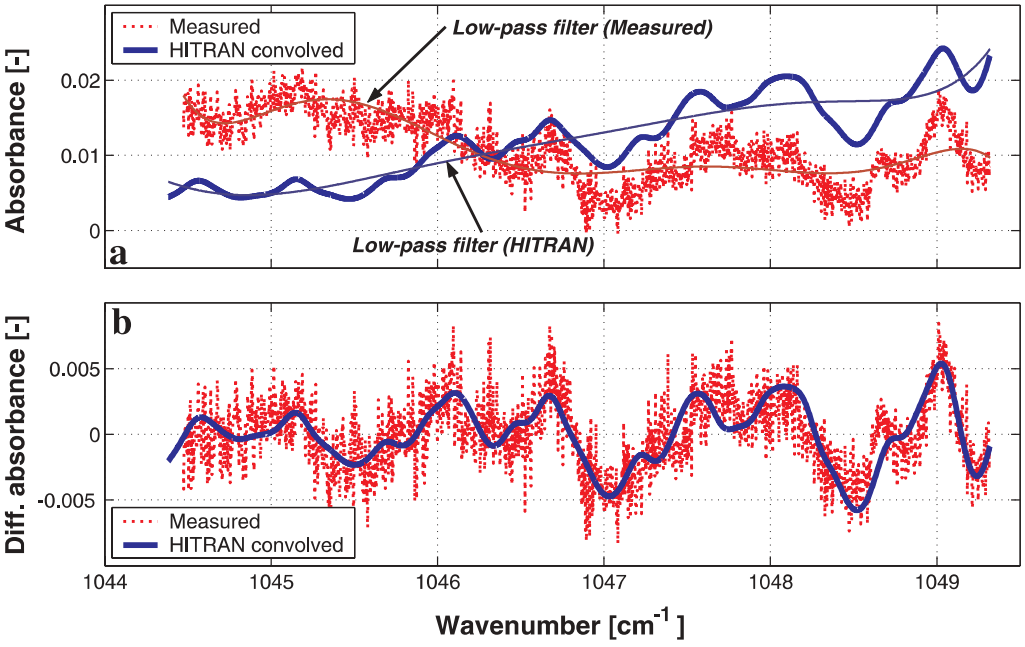

FIGURE 4 Application of the differential absorption method to the QCL spectra at 28 ppm m O_3. **a** The measured and calculated absorption spectra are shown along with their corresponding polynomial low-pass filters *(thin lines)*. **b** The measured differential absorption spectrum is in good agreement with the HITRAN-based calculation

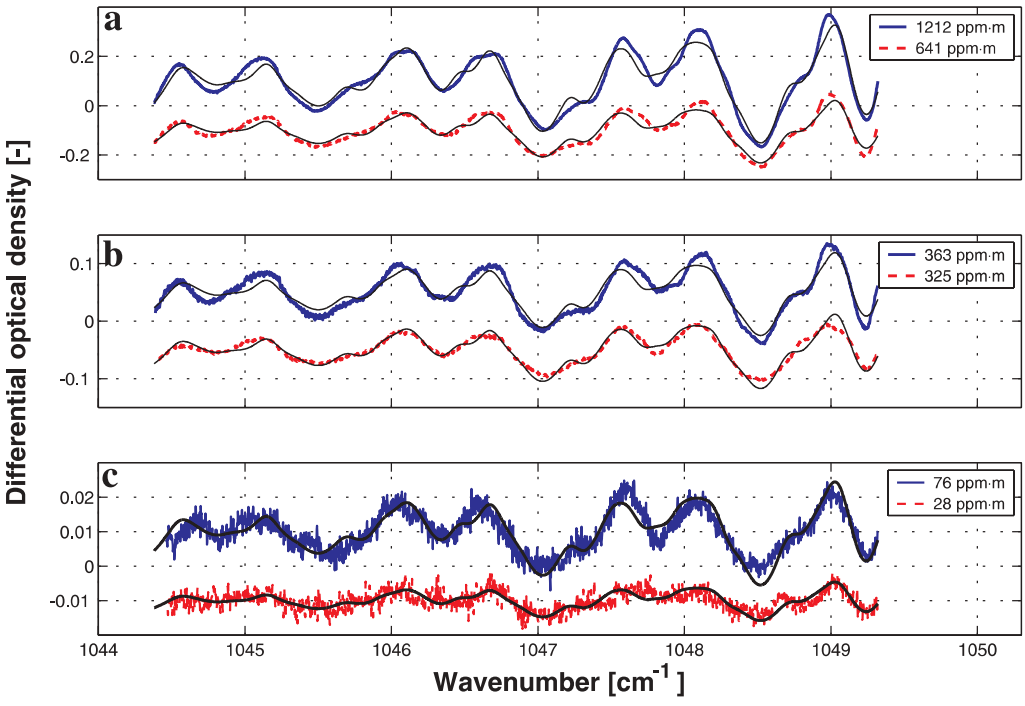

FIGURE 5 Measured *(thick lines)* and HITRAN-based calculated *(thin lines)* QCL differential absorption spectra at **a** high, **b** moderate, and **c** low ozone column densities. Measured and calculated spectra were *vertically* displaced for visualization purposes

assumption on the actual baseline is required. The differential optical density, ΔD, is calculated as the LP-filter subtracted optical density:

$$\Delta D\left(\tilde{\nu}\right) = D\left(\tilde{\nu}\right) - f\left(D\left(\tilde{\nu}\right)\right) \tag{3}$$

The LP-filters shown in Fig. 4a are plain 7^{th} degree fitting polynomials. Subtraction of these trend curves leads to a highly improved agreement between measured and calculated absorbances (see Fig. 4b).

The procedure described above is the basis of the DOAS technique [6, 7], developed and successfully applied since the late seventies to the detection over long open paths of important trace gases in the UV-visible, frequently at the sub-ppb level. The differential absorption method makes possible the retrieval of concentrations in open path conditions, for which the light source spectra is known but the actual baseline spectra cannot be determined, particularly in the UV, where Mie attenuation is very important.

The resulting QCL differential absorption spectra along with their theoretical counterparts are shown in Fig. 5. Good agreement between measurements and calculations is observed for all the column densities above 28 ppm m, which confirms that the discrepancies observed in Fig. 3 are due to baseline inaccuracies. A closer look at Fig. 5 reveals that the differential spectra are slightly noisier at lower wavenumbers,

i.e. at higher temperatures. This wavelength dependence of the SNR is explained by the significant decrease of the laser power (∼ 70%) between −35 and +35 °C.

We investigated two approaches for concentration retrieval from both absolute and differential absorption spectra: comparison with a high SNR reference spectrum (D_0 and ΔD_0, for absolute and differential spectra, respectively) and linearization of the BLB law. The first approach assumes linear dependence of the absorbance, and consequently of the differential absorbance, with the column density. Due to the finite linewidth of the QCL, this assumption is strictly valid only at column densities approaching that of the reference spectrum, $(cL)_0$. The column density ratio, $a \cong (cL)/(cL)_0$, is retrieved by a zero offset, least squares linear fitting of the measured spectra to the reference spectra, whether absolute, $D(\tilde{\nu}) \cong aD_0(\tilde{\nu})$, or differential, $\Delta D(\tilde{\nu}) \cong a\Delta D_0(\tilde{\nu})$. The concentrations shown in Fig. 6 were calculated using the highest column density (1212 ± 34 ppm m) spectrum as reference (a Savitzky–Golay low-pass filter was applied previous utilization).

The second concentration retrieval approach assumes that the optical density, D_H, is small enough ($D_H \cong 1 - \tau_H$) to be appropriately expressed as,

$$D_H(\tilde{\nu}) \cong \sigma_H(\tilde{\nu})\, cL \tag{4}$$

where $\sigma_H = \sigma \otimes H$ is the convolution product of the cross section with the average QCL lineshape. The linearization above is numerically valid within ±1% for (relative) absorptances below 17%, an inherently fulfilled condition in open path spectroscopy of trace gases. Column densities are directly retrieved ($b \cong cL$) by least squares linear fitting of the convolved cross section, whether to the absolute, $D(\tilde{\nu}) \cong b\sigma_H(\tilde{\nu}) + b_0$, or to the differential absorbance, $\Delta D(\tilde{\nu}) \cong b\Delta\sigma_H(\tilde{\nu})$ (the b_0 coefficient is intended at correcting a constant baseline offset). The differential convolved cross section, $\Delta\sigma_H$,

$$\Delta\sigma_H(\tilde{\nu}) = \sigma_H(\tilde{\nu}) - f(\sigma_H(\tilde{\nu})) \tag{5}$$

is calculated by subtraction of an absorbance-homologous LP-filter (a 7^{th} degree polynomial in our case). Results are shown in Fig. 6.

The most accurate column densities were retrieved from absolute spectra using the highest column density spectrum as reference. Discrepancies are typically lower than ±2% (above LDL), i.e. within the uncertainty of the DOAS measurements. On the other hand, retrieval from absolute absorption spectra with the convolved cross section yields rather accurate (∼ 9% underestimation) column densities above ∼ 300 ppm m only. At lower column densities unmatched baseline features lead to very inaccurate (60% underestimation) or even negative column densities (see Fig. 6a). In contrast, the two approaches produce similar results when applied to differential spectra, typically with ±15% accuracy (above LDL). Moreover, fitting to the cross section yields more accurate results near the detection limit (see Fig. 6b). Below ∼ 80 ppm m, differential spectra were found to yield more precise (±1%) column densities than absolute spectra (±3% precision).

The detection limits of the absolute and differential methods were estimated using the root-mean-square (RMS) of the residuum (δ) between observed and calculated absorbances ($\delta_D = D - D_H$ or $\delta_{\Delta D} = \Delta D - \Delta D_H$) as a measure

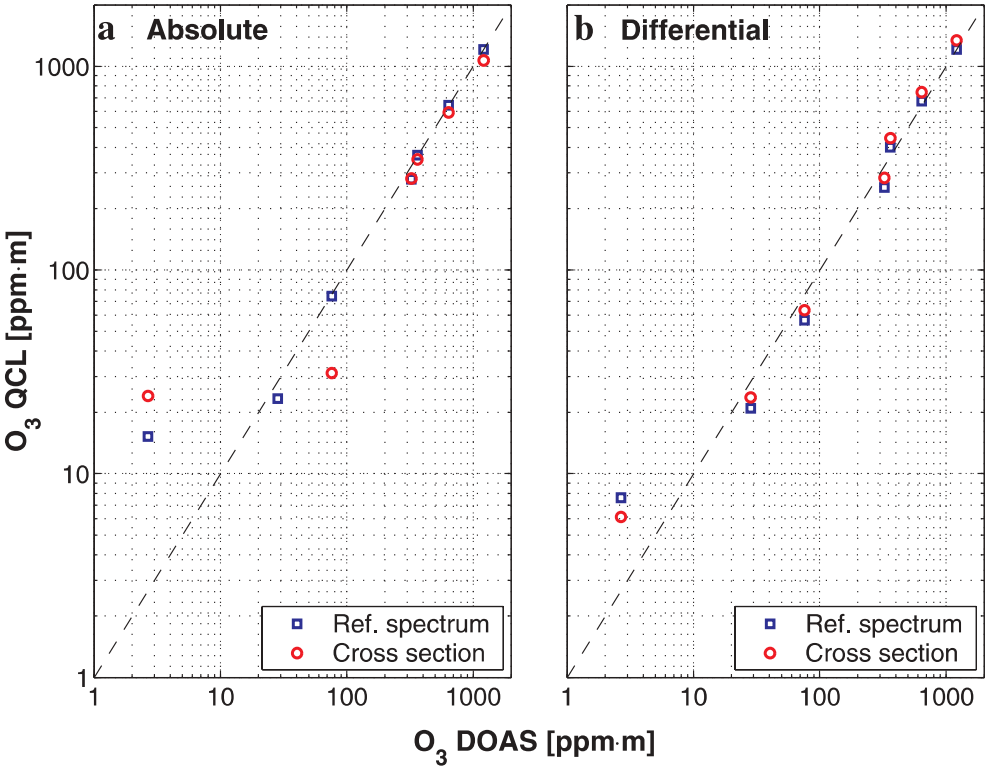

FIGURE 6 Comparison of ozone column densities retrieved from QCL **a** absolute and **b** differential absorption spectra to the QCL-equivalent reference values (DOAS). Retrievals using a high SNR spectrum as reference and with the convolved cross section are presented. The QCL and DOAS absorption pathlengths were 192 cm and 100 cm, respectively

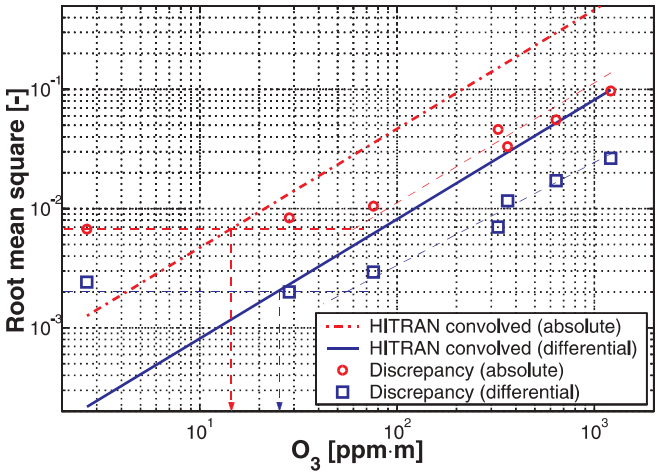

FIGURE 7 Root mean square of the theoretical spectral signal (HITRAN convolved) and of the discrepancy of measurements to the theoretical values as a function of the O_3 column density. Signal and discrepancy are given for QCL absolute and differential absorption spectra. The lowest detectable absorbances (RMS) and column densities are estimated for a SNR of 1

of the spectral noise. The LDLs are calculated as the column densities at which the expected spectral signal (RMS of D_H or ΔD_H) equals the discrepancy RMS, i.e. for a SNR of 1. The lowest detectable column densities with the absolute and differential methods are estimated at 14 ppm m and 25 ppm m, respectively (see Fig. 7). These values correspond to lowest detectable absolute and differential QCL absorptions (RMS) of 7×10^{-3} and 2×10^{-3}, respectively. A close look at the 28 ppm m O_3 differential spectrum (see Fig. 4b) indicates that the actual LDL of the differential method is probably better than that estimated from the RMS discrepancy analysis. This absorption spectrum is clearly above the LDL although it shows a peak-to-peak noise level of $\sim 5 \times 10^{-3}$ absorbance units. This fairly high noise level is due to the low pulse averaging rate achieved in the experiment ($\sim$ 20 Hz effective).

The resulting differential to absolute LDL ratio of 1.8 is well below the theoretical ratio of 5.8, estimated as the absolute to differential cross section ratio (RMS),

$$\frac{\mathrm{LDL_{DIFF}}}{\mathrm{LDL_{ABS}}} \approx \frac{\mathrm{RMS}\ (\sigma_H)}{\mathrm{RMS}\ (\Delta\sigma_H)} \qquad (6)$$

This implies that the LDL achieved with absolute absorption spectra is three times higher than expected. This reduced performance mainly stems from inaccuracy in the baseline determination.

5 Conclusions and perspectives

Our O_3 measurements covered a $\sim$ 3-decade column density range (3–1212 ppm m). Accurate concentrations ($\pm$2%) were retrieved from QCL absolute absorption spectra using a high SNR spectrum (1212 $\pm$ 34 ppm m) as reference. The differential method was found to be less accurate ($\pm$15%) but on average more reliable and precise at lower concentration levels ($<$ 80 ppm m).

For wavelength mapping purposes, we measured the heat sink temperature dependence on the duty conditions. This dependence can be satisfactorily explained considering the transfer of heat from the QCL heterostructure to the sink. A parametric extension of this analysis should allow representing a QCL calibration curve family with a single, parametric-dependent temperature-to-wavelength calibration curve.

A detailed mapping of the linewidth dependence on the duty conditions (dc and i/i_{th}) is important concerning the wavelength-dependent convolution of calculated cross sections. This procedure is particularly important for the retrieval of analytically difficult (adsorptive or reactive) species without requiring previous laboratory reference spectra measurements. We observed a negative dependence of the linewidth with temperature. This finding deserves further experimental investigation, preferably with a high-resolution FTIR spectrometer.

A fairly large spectral range is required for unambiguous identification of species at atmospheric pressure due to line broadening. We obtained spectra of up to 7 cm^{-1} by temperature tuning at $\sim$ 0.3 cm^{-1}/min. This slow scanning speed is obviously unsuitable for open path measurements due to the dynamic nature of the atmosphere. We have recently attained scanning rates of $\sim$ 2.5 cm^{-1}/min using a single, non-controlled temperature step with promising spectral results (fast scanning wavelength reproducibility have been extensively demonstrated – the work of Beyer et al. [16] is a remarkable example). Moreover, operation with shorter QCL pulses ($\sim$ 20 ns) should significantly improve the spectral resolution thus allowing for unambiguous identification of ozone using a narrower wavelength range ($\sim$ 3 cm^{-1}). Appropriate scanning times ($\sim$ 1–2 min) could be achieved this way.

Improving the current differential absorption LDL (25 ppm m) to the level of commercial DOAS systems ($\sim$ 2 ppm m) would require increasing almost 160-fold the QCL pulse averaging rate. In addition, open-path detection would necessitate decreasing almost 20-fold the current wavelength scanning time. This combination of requirements implies an effective pulse averaging rate of $\sim$ 4 kHz for an $\sim$ 300 effective data point averaged spectrum scanned in $\sim$ 1 min. We are currently developing a synchronous (gated) sampling board that is expected to allow for pulse averaging at up to $\sim$ 100 kHz. We intend to use two pairs of these boards for the simultaneous averaging of the signal peak and baseline of both, reference and transmitted pulses. Provided that the averaging rate is significantly improved, a reduction of the linewidth should render additional improvement of the SNR ($\sim$ 50% reduction of the linewidth yields $\sim$ 30% increase of the $\Delta\sigma_H$ RMS).

Our results demonstrate the applicability of the differential method to QCL spectroscopy at atmospheric pressure and facilitate its application to open-path spectroscopic detection of trace gases. We have recently performed preliminary open-air QCL absorption measurements over a 460 m atmospheric path using a monostatic (emitter-retroreflector-receiver) configuration, and obtained return signals of good intensity and highly structured spectra.

ACKNOWLEDGEMENTS We gratefully acknowledge Alpes Lasers for kindly providing us with the QCL used in this investigation, particularly to A. Müller for his cooperation and valuable discussions. EPFL/LPAS research was financially supported by EPFL/VPR, NCCR

(Quantum Photonics Grant), ICSC-World Laboratory (Project LAND-14), and Thermo Electron Air Quality Inc.

REFERENCES

1 S. Perego: Meteor. Atmos. Phys. **70**, 43 (1999)
2 P. Thunis, A. Clappier: Mon. Wea. Rev. **128**, 3236 (2000)
3 O. Couach, I. Balin, R. Jiménez, P. Ristori, S. Perego, F. Kirchner, V. Simeonov, B. Calpini, H. van den Bergh: Atmos. Chem. Phys. **3**, 549 (2003)
4 R. Jiménez, T. Iannone, H. van den Bergh, B. Calpini, D. Kita: A&WMA 93rd Annual Conf. & Exhib., paper 830 (18-22 June 2000)
5 M.W. Sigrist (Ed.): *Air monitoring by spectroscopic techniques* (Wiley, NY 1993)
6 U. Platt: *Differential optical absorption spectroscopy*. (In M.W. Sigrist, *Air monitoring by spectroscopic techniques*, Wiley, NY 1993) p. 27
7 J. Stutz, U. Platt: Appl. Opt. **35**, 6041 (1996)
8 J. Faist, F. Capasso, D.L. Sivco, C. Sirtori, A.L. Hutchinson, A.Y. Cho: Science **264**, 553 (1994)
9 C. Gmachl, A. Straub, R. Colombelli, F. Capasso, D.L. Sivco, A.M. Sergent, A.Y. Cho: IEEE J. Quantum Electron. **QE-38**, 569 (2002)
10 C.R. Webster, G.J. Flesch, D.C. Scott, J.E. Swanson, R.D. May, W.S. Woodward, C. Gmachl, F. Capasso, D.L. Sivco, J.N. Baillargeon, A.L. Hutchinson, A.Y. Cho: Appl. Opt. **40**, 321 (2001)
11 A.A. Kosterev, F.K. Tittel, R. Köhler, C. Gmachl, F. Capasso, D.L. Sivco, A.Y. Cho, S. Wehe, M.G. Allen: Appl. Opt. **41**, 1169 (2002)
12 A.A. Kosterev, R.F. Curl, F.K. Tittel, M. Rochat, M. Beck, D. Hofstetter, J. Faist: Appl. Phys. B **75**, 351 (2002)
13 D.D. Nelson, J.H. Shorter, J.B. McManus, M.S. Zahniser: Appl. Phys. B **75**, 343 (2002)
14 D. Hofstetter, M. Beck, J. Faist, M. Nägele, M.W. Sigrist: Opt. Lett. **26**, 887 (2001)
15 S. Schilt, L. Thévenaz, E. Courtois, P.A. Robert: Spectrochim. Acta A **58**, 2533 (2002)
16 T. Beyer, M. Braun, A. Lambrecht: J. Appl. Phys. **93**, 3158 (2003)
17 J.M. Flaud, R. Bacis: Spectrochim. Acta A **54**, 3 (1998)
18 D. Daumont, J. Brion, J. Charbonnier, J. Malicet: J. Atmos. Chem. **15**, 145 (1992)
19 V.M. Devi, D.C. Benner, C.P. Rinsland, M.A.H. Smith, D.S. Parmar: Recent Res. Devel. Geophys. Res. **1**, 119 (1996)
20 L.S. Rothman, C.P. Rinsland, A. Goldman, S.T. Massie, D.P. Edwards, J.M. Flaud, A. Perrin, C. Camy-Peyret, V. Dana, J.Y. Mandin, J. Schroeder, A. McCann, R.R. Gamache, R.B. Wattson, K. Yoshino, K.V. Chance, K.W. Jucks, L.R. Brown, V. Nemtchinov, P. Varanasi: J. Quant. Spectrosc. Radiat. Transfer **60**, 665 (1998)
21 C. Claveau, M. Lepère, G. Dufour, A. Valentin, A. Henry, C. Camy–Peyret, D. Hurtmans: Spectrochim. Acta A **58**, 2313 (2002)
22 A. Wacker, S.C. Lee: Physica B **314**, 327 (2002)
23 V.B. Gorfinkel, S. Luryi, B. Gelmont: IEEE J. Quantum Electron. **QE-32**, 1995 (1996)